Electronic Supplementary Material (ESI) for Nanoscale.

Supporting information

The supporting information consists of 6 sections. The list of the sections and a brief description of each section follows.

I. Theorectical Calculation of Oxide Thickness Dependence of SPP Wavelength
1. The scheme of the boundary conditions and the results of the theoretical calculation of the oxide thickness dependence of the wavelength of the SPP propagating at the SiO_2/Ag interface.
2. The derivation of the ideal zone width for a π-phase shift for 2-level Fresnel phase zone pad structures.

II. Up-conversion Fluorescence Microscope System
Schematics of the experimental setup for the up-conversion fluoresence microscope.

III. Scheme of Intensity Line Profile Extraction
The cooridnate system and the orientation of the line segments where the intensity line profiles were extracted from the simulation or experimental images.

IV. Design of 4-level FPZP Structures and Comparison of SPP Focusing Properties
Design of the 4-level FPZP structures and the comparison of the SPP focusing of the 4-level FPZP structures with that of the 2-level FPZP structures.

V. Focusing Efficiency of Optimal FPZP structures
The focusing efficiency of the optimal 2-level and the 4-level FPZP structures.

VI. Longevity of FPZP structures
The comparison of the SPP focusing of the FPZP structure right after fabrication and that after the devices being stored in ambient environment over an extended period of time.

I. Theorectical Calculation of Oxide Thickness Dependence of SPP Wavelength

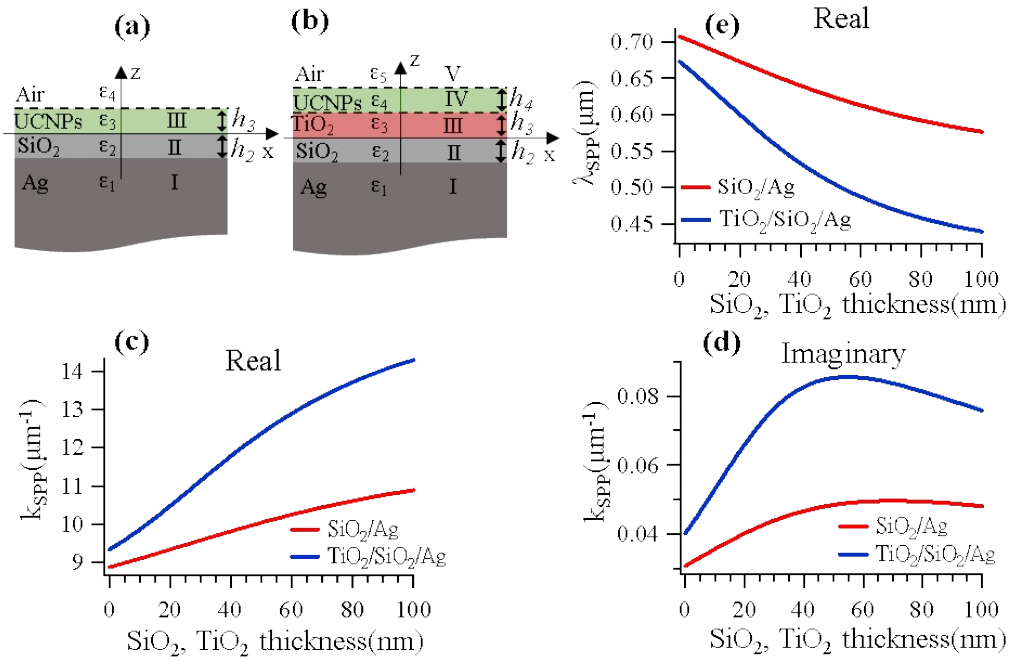

Figure S1. Theoretical analysis of SPP wavevector as a function of SiO_2 and TiO_2 thickness above the SiO_2/Ag interface. The wavelength in vacuum is 793 nm. (a) The boundary conditions for SPP propagation at the SiO_2/Ag interface in the experiment, where the SiO_2/Ag interface was covered with a layer of UCNPs. ε_1, ε_2, ε_3, and ε_4 represent the dielectric constant of the Ag (labeled as layer I), the SiO_2 layer (layer II), the UCNP layer (layer III), and the Air (layer IV), respectively. (b) The boundary conditions for SPP propagation at the TiO_2/ 20-nm-SiO_2/Ag interface in the experiment, where the TiO_2 layer was also covered with a layer of UCNPs. ε_1, ε_2, ε_3, ε_4, and ε_5 represent the dielectric constant of the Ag layer (layer I), the SiO_2 layer (layer II), the TiO_2 layer (layer III), the UCNP layer (layer IV), and Air (layer V), respectively. In both (a) and (b) we approximate the UCNP layer with a uniform 50-nm-thick layer of the host materials of the UCNPs, i.e. $NaYF_4$. (c) and (d) show the real and imaginary components of the SPP wavevector as a function of the oxide thickness, respectively. The red solid curves in (c) and (d) represent, respectively, the real and the imaginary components of the SPP wavevector under the boundary condition shown in (a) plotted as a function of the SiO_2 thickness. In the experiment the thickness of the SiO_2 layer thickness was fixed to 20 nm. The blue solid curves in (c) and (d) represent, respectively, the real and the imaginary components of the SPP wavevector plotted as a function of TiO_2 thickness under the boundary condition shown in (b), and in the experiment the TiO_2 layer thickness was fixed to 40 nm. (e) The SPP wavelengths derived from the real component of the SPP wavevector in (c) plotted as a function of the oxide thickness.

The equations derived from Maxwell's equations and boundary condition in (a) for finding the SPP wavevector k_x are the following:

$$a_2^2 a_3^2 \left(\frac{k_{z_1}}{\varepsilon_1}-\frac{k_{z_2}}{\varepsilon_2}\right)\left(\frac{k_{z_3}}{\varepsilon_3}-\frac{k_{z_4}}{\varepsilon_4}\right)\left(\frac{k_{z_2}}{\varepsilon_2}+\frac{k_{z_3}}{\varepsilon_3}\right)+a_2^2\left(\frac{k_{z_1}}{\varepsilon_1}-\frac{k_{z_2}}{\varepsilon_2}\right)\left(\frac{k_{z_3}}{\varepsilon_3}+\frac{k_{z_4}}{\varepsilon_4}\right)\left(\frac{k_{z_2}}{\varepsilon_2}-\frac{k_{z_3}}{\varepsilon_3}\right)$$
$$+a_3^2\left(\frac{k_{z_1}}{\varepsilon_1}+\frac{k_{z_2}}{\varepsilon_2}\right)\left(\frac{k_{z_3}}{\varepsilon_3}-\frac{k_{z_4}}{\varepsilon_4}\right)\left(\frac{k_{z_2}}{\varepsilon_2}-\frac{k_{z_3}}{\varepsilon_3}\right)+\left(\frac{k_{z_1}}{\varepsilon_1}+\frac{k_{z_2}}{\varepsilon_2}\right)\left(\frac{k_{z_3}}{\varepsilon_3}+\frac{k_{z_4}}{\varepsilon_4}\right)\left(\frac{k_{z_2}}{\varepsilon_2}+\frac{k_{z_3}}{\varepsilon_3}\right)=0 \quad \text{(S1)}$$

$$k_{z_1}^2+k_x^2=\varepsilon_1\left(\frac{\omega}{c}\right)^2 \quad \text{(S2)}$$

$$k_{z_2}^2+k_x^2=\varepsilon_2\left(\frac{\omega}{c}\right)^2 \quad \text{(S3)}$$

$$k_{z_3}^2+k_x^2=\varepsilon_3\left(\frac{\omega}{c}\right)^2 \quad \text{(S4)}$$

$$k_{z_4}^2+k_x^2=\varepsilon_4\left(\frac{\omega}{c}\right)^2 \quad \text{(S5)}$$

, where $a_2=e^{ik_{z_2}h_2}$,and h_2 is thickness of the SiO_2 layer; $a_3=e^{ik_{z_3}h_3}$,and h_3 = 50 nm for the effective thickness of the UCNP layer; k_{z1}, k_{z2}, k_{z3}, k_{z4} are the z-components of the wave vectors of the electro-magnetic fields in regions I, II, III, and IV, respectively.

The equations derived from Maxwell's equations and boundary condition in (b) for finding the SPP wavevector k_x are the following:

$$-a_4a_3a_2\left(\frac{k_{z_4}}{\varepsilon_4}-\frac{k_{z_5}}{\varepsilon_5}\right)\left(\frac{k_{z_3}}{\varepsilon_3}+\frac{k_{z_4}}{\varepsilon_4}\right)\left(\frac{k_{z_2}}{\varepsilon_2}+\frac{k_{z_3}}{\varepsilon_3}\right)\left(\frac{k_{z_1}}{\varepsilon_1}-\frac{k_{z_2}}{\varepsilon_2}\right)$$
$$-\frac{1}{a_4}a_3a_2\left(\frac{k_{z_4}}{\varepsilon_4}+\frac{k_{z_5}}{\varepsilon_5}\right)\left(\frac{k_{z_3}}{\varepsilon_3}-\frac{k_{z_4}}{\varepsilon_4}\right)\left(\frac{k_{z_2}}{\varepsilon_2}+\frac{k_{z_3}}{\varepsilon_3}\right)\left(\frac{k_{z_1}}{\varepsilon_1}-\frac{k_{z_2}}{\varepsilon_2}\right)$$
$$-a_4\frac{1}{a_3}a_2\left(\frac{k_{z_4}}{\varepsilon_4}-\frac{k_{z_5}}{\varepsilon_5}\right)\left(\frac{k_{z_3}}{\varepsilon_3}-\frac{k_{z_4}}{\varepsilon_4}\right)\left(\frac{k_{z_2}}{\varepsilon_2}-\frac{k_{z_3}}{\varepsilon_3}\right)\left(\frac{k_{z_1}}{\varepsilon_1}-\frac{k_{z_2}}{\varepsilon_2}\right)$$
$$-\frac{1}{a_4}\frac{1}{a_3}a_2\left(\frac{k_{z_4}}{\varepsilon_4}+\frac{k_{z_5}}{\varepsilon_5}\right)\left(\frac{k_{z_3}}{\varepsilon_3}+\frac{k_{z_4}}{\varepsilon_4}\right)\left(\frac{k_{z_2}}{\varepsilon_2}-\frac{k_{z_3}}{\varepsilon_3}\right)\left(\frac{k_{z_1}}{\varepsilon_1}-\frac{k_{z_2}}{\varepsilon_2}\right)$$
$$-a_4a_3\frac{1}{a_2}\left(\frac{k_{z_4}}{\varepsilon_4}-\frac{k_{z_5}}{\varepsilon_5}\right)\left(\frac{k_{z_3}}{\varepsilon_3}+\frac{k_{z_4}}{\varepsilon_4}\right)\left(\frac{k_{z_2}}{\varepsilon_2}-\frac{k_{z_3}}{\varepsilon_3}\right)\left(\frac{k_{z_1}}{\varepsilon_1}+\frac{k_{z_2}}{\varepsilon_2}\right)$$
$$-\frac{1}{a_4}a_3\frac{1}{a_2}\left(\frac{k_{z_4}}{\varepsilon_4}+\frac{k_{z_5}}{\varepsilon_5}\right)\left(\frac{k_{z_3}}{\varepsilon_3}-\frac{k_{z_4}}{\varepsilon_4}\right)\left(\frac{k_{z_2}}{\varepsilon_2}-\frac{k_{z_3}}{\varepsilon_3}\right)\left(\frac{k_{z_1}}{\varepsilon_1}+\frac{k_{z_2}}{\varepsilon_2}\right)$$
$$-a_4\frac{1}{a_3}\frac{1}{a_2}\left(\frac{k_{z_4}}{\varepsilon_4}-\frac{k_{z_5}}{\varepsilon_5}\right)\left(\frac{k_{z_3}}{\varepsilon_3}-\frac{k_{z_4}}{\varepsilon_4}\right)\left(\frac{k_{z_2}}{\varepsilon_2}+\frac{k_{z_3}}{\varepsilon_3}\right)\left(\frac{k_{z_1}}{\varepsilon_1}+\frac{k_{z_2}}{\varepsilon_2}\right)$$
$$-\frac{1}{a_4}\frac{1}{a_3}\frac{1}{a_2}\left(\frac{k_{z_4}}{\varepsilon_4}+\frac{k_{z_5}}{\varepsilon_5}\right)\left(\frac{k_{z_3}}{\varepsilon_3}+\frac{k_{z_4}}{\varepsilon_4}\right)\left(\frac{k_{z_2}}{\varepsilon_2}+\frac{k_{z_3}}{\varepsilon_3}\right)\left(\frac{k_{z_1}}{\varepsilon_1}+\frac{k_{z_2}}{\varepsilon_2}\right)=0 \quad \text{(S6)}$$

$$k_{z_1}^2 + k_x^2 = \varepsilon_1 \left(\frac{\omega}{c}\right)^2 \quad \text{(S7)}$$

$$k_{z_2}^2 + k_x^2 = \varepsilon_2 \left(\frac{\omega}{c}\right)^2 \quad \text{(S8)}$$

$$k_{z_3}^2 + k_x^2 = \varepsilon_3 \left(\frac{\omega}{c}\right)^2 \quad \text{(S9)}$$

$$k_{z_4}^2 + k_x^2 = \varepsilon_4 \left(\frac{\omega}{c}\right)^2 \quad \text{(S10)}$$

$$k_{z_5}^2 + k_x^2 = \varepsilon_5 \left(\frac{\omega}{c}\right)^2 \quad \text{(S11)}$$

, where $a_2 = e^{ik_{z_2}h_2}$, and h_2 = 20 nm for thickness of the SiO_2 layer; $a_3 = e^{ik_{z_3}h_3}$, and h_3 is thickness of the TiO_2 layer; $a_4 = e^{ik_{z_4}h_4}$, and h_4 = 50 nm for the effective thickness of the UCNP layer; k_{z1}, k_{z2}, k_{z3}, k_{z4}, k_{z5} are the z-components of the wave vectors of the electro-magnetic fields in regions I, II, III, and IV, V respectively.

Ideal zone width of the FPZP structures

The design principle of the 2-level FPZP structures follows that of the Fresnel phase zone plate in optics. The incident SPP is assumed to be collimated and passing the FPZP structure at normal incidence, with minimal scattering and no dissipation, and the zone width ***d*** is designed to produce a π-radian phase difference between the wavefront at neighboring zones due to the difference in the SPP wavelengths, i.e. $\lambda_{SPP,SiO2/Ag}$ = 675 nm, and $\lambda_{SPP,TiO2/SiO2/Ag}$=536 nm. Therefore, the ideal zone width $\boldsymbol{d_0}$ can be obtained with the following calculation.

$$d_0 \cdot \frac{2\pi}{\lambda_{SPP,TiO2/SiO2/Ag}} - d_0 \cdot \frac{2\pi}{\lambda_{SPP,SiO2/Ag}} = \pi$$

$$\Rightarrow d_0 = \frac{\pi}{\frac{2\pi}{536nm} - \frac{2\pi}{675nm}} \cong 1.30um$$

II. Up-conversion Fluorescence Microscope System

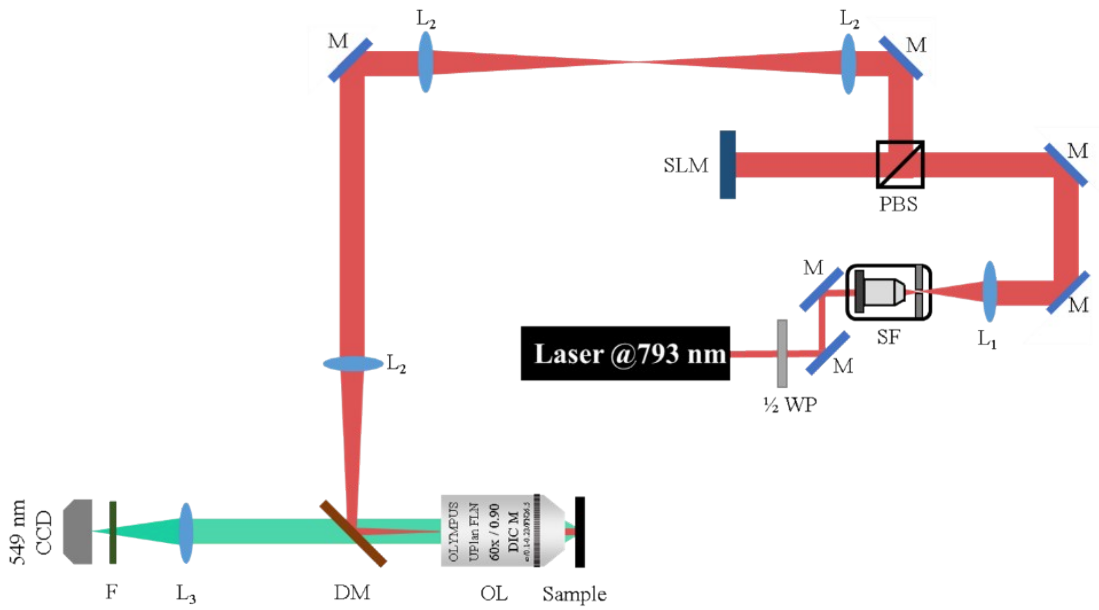

Figure S2. The schematics of the experimental setup of the up-conversion fluorescent microscopy. The list of the optical components labeled in the schematics follows.

M : Mirror

½WP: ½ waveplate (800 nm)

L_1: Lens (f = 100 mm)

L_2: Lens (f = 300 mm)

L_3: Lens (f = 200 mm)

SF: Spatial Filter

OL: Objective Lens (60x / NA 0.9)

PBS: Polarizing Beam-splitter

SLM: Spatial Light Modulator

DM: Dichroic Mirror (650 nm short-pass) (>50%)

F: Bandpass Filter (549.0/16.7 nm) (>95%)

III. Scheme of Intensity Line Profile Extraction

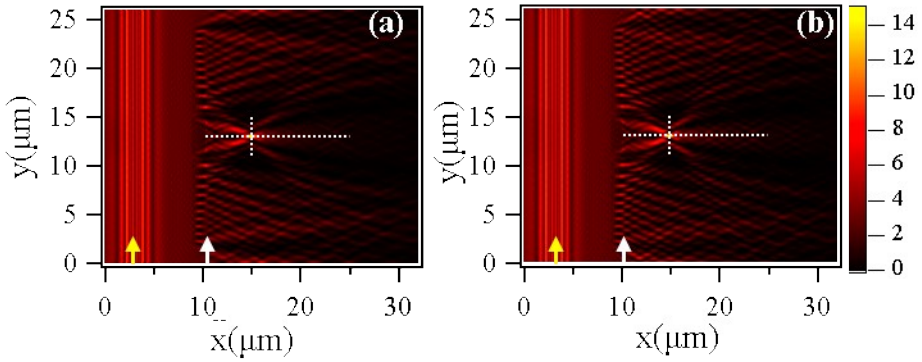

Figure S3. (a), (b) The horizontal and the vertical line segments where the longitudinal and transverse E-field intensity line profiles in Fig. 2(c) and 2(d) are extracted, respectively. The yellow arrow indicates the position of the coupling grating, and the white arrow indicate the position of the right edge of the FPZP structure.

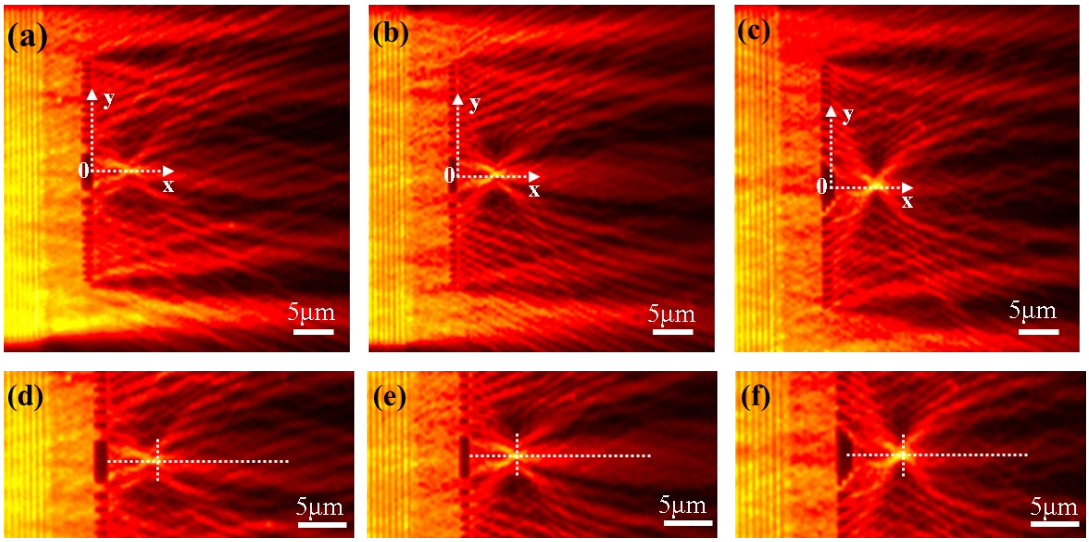

Figure S4. (a), (b), (c) The coordinate system for extracting the fluorescent intensity line profiles from the images shown in Figure 4 (a), (b) and Figure 6(a) respectively. (d), (e) and (f) The horizontal and vertical line segments indicate where the longitudinal and the transverse fluorescent intensity line profiles in Fig. 4(a), (b) and Fig. 6(a) are extracted, respectively.

IV. Design of 4-level FPZP Structures and the Comparison of SPP Focusing Properties

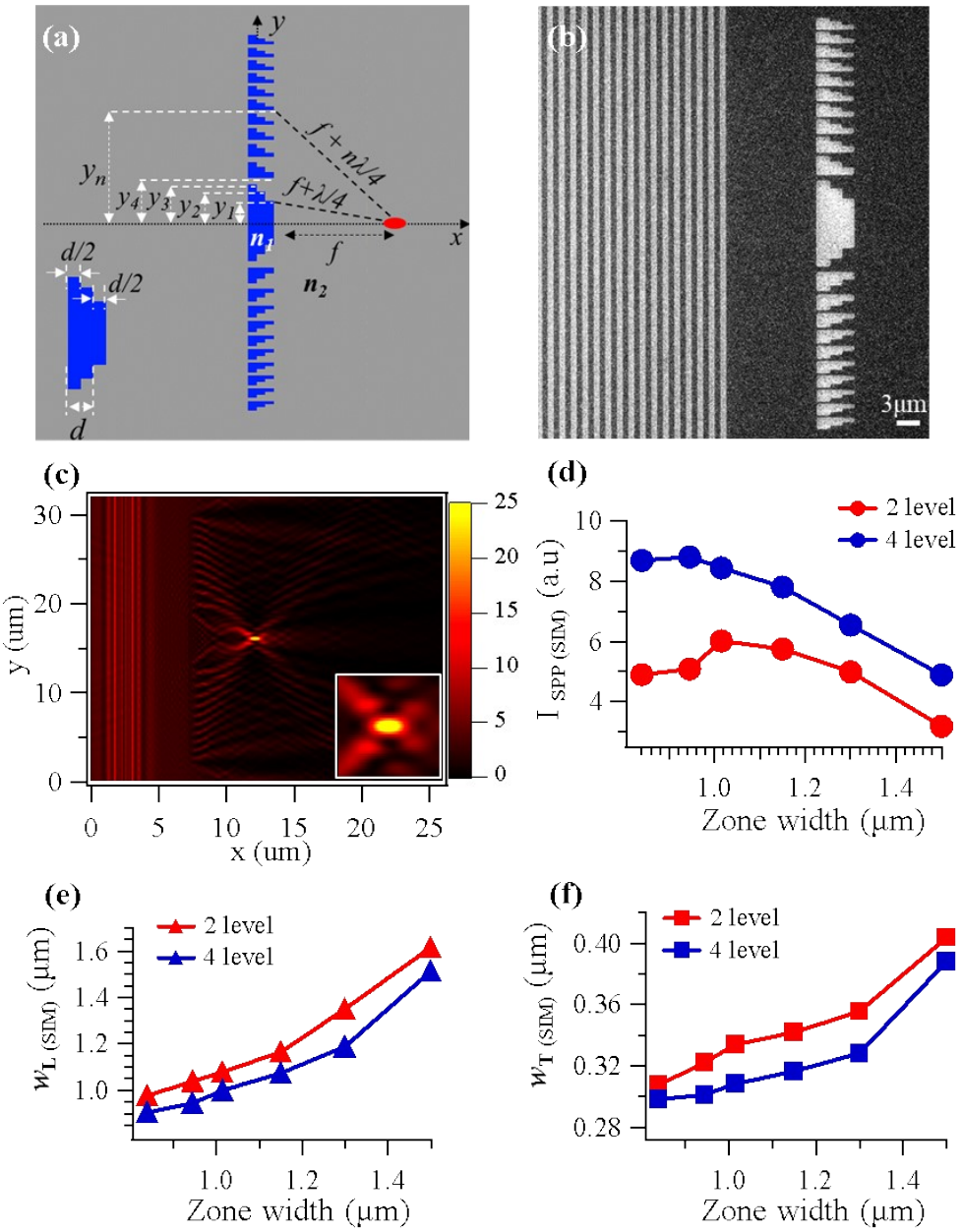

Figure S5. (a) The schematics of the 4-level FPZP structure design. The 4-level FPZP structure is designed to have the zone width of 0, ***d***/2, ***d*** and 3***d*** /2 for each level in a modulo-2π zone structure. This results in a π/2 phase shift between the adjacent zones. The vertical coordinate y_n's are calculated with the following equations:

$$y_n = \sqrt{\frac{|n| f \lambda_{sio_2/Ag}}{2} + \frac{n^2 \lambda_{sio_2/Ag}^2}{16}},$$

where $\lambda_{sio2/Ag}$ = 675 nm, ***n*** is the number index of each zone. (b) SEM image of the 4-level FPZP with focal length ***f*** = 5 μm. (c) The FDTD simulated E-field intensity

distribution of the SPP focusing with the 4-level FPZP structure at 5-μm focal length. (d), (e), (f) The comparison of the simulated SPP focusing with the 2-level FPZP strictures and that with the 4-level FPZP structures. (d) The normalized peak fluorescent intensity at the SPP focal spot as a function of the zone width ***d***. (e) and (f) show, respectively, w_L, and w_T as a function of the zone width ***d***.

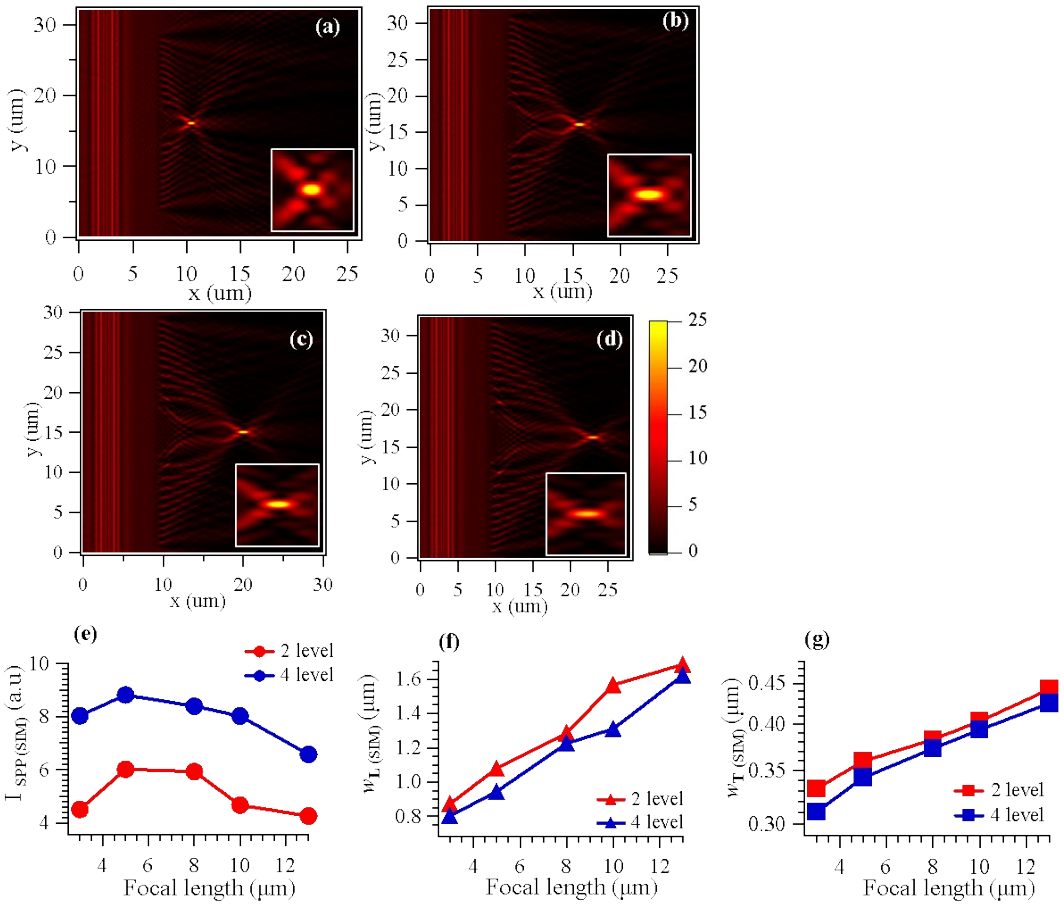

Figure S6. The FDTD simulated E-field intensity image of the SPP focusing with the 4-level FPZP with the focal length of 3 μm, 8 μm, 10 μm and 13 μm in (a), (b), (c), and (d), respectively. (e), (f), (g) The comparison of SPP focusing with 2-level and 4-level of FPZP structure in FDTD simulation. (e) The plot of the normalized intensity as a function of focal length with the optimal zone width in each focal length ***f***. (f), (g) The plot of focus spot size w_L and w_T as a function of focal length with the optimal zone width in each focal length ***f***, respectively.

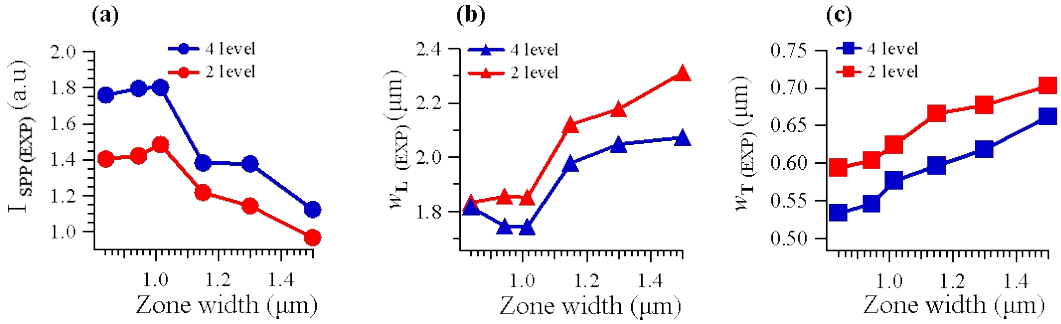

Fig. S7 Comparison between SPP focusing at 5μm focal length with 4-level FPZP structures and that with 2-level FPZP structures in experiment. (a) The normalized peak fluorescent focal spot peak intensity a function of the zone width ***d***. (b) and (c) show, respectively, the focus spot size w_L and w_T as a function of the zone width ***d***.

V. Focusing Efficiency of Optimal FPZP Structures

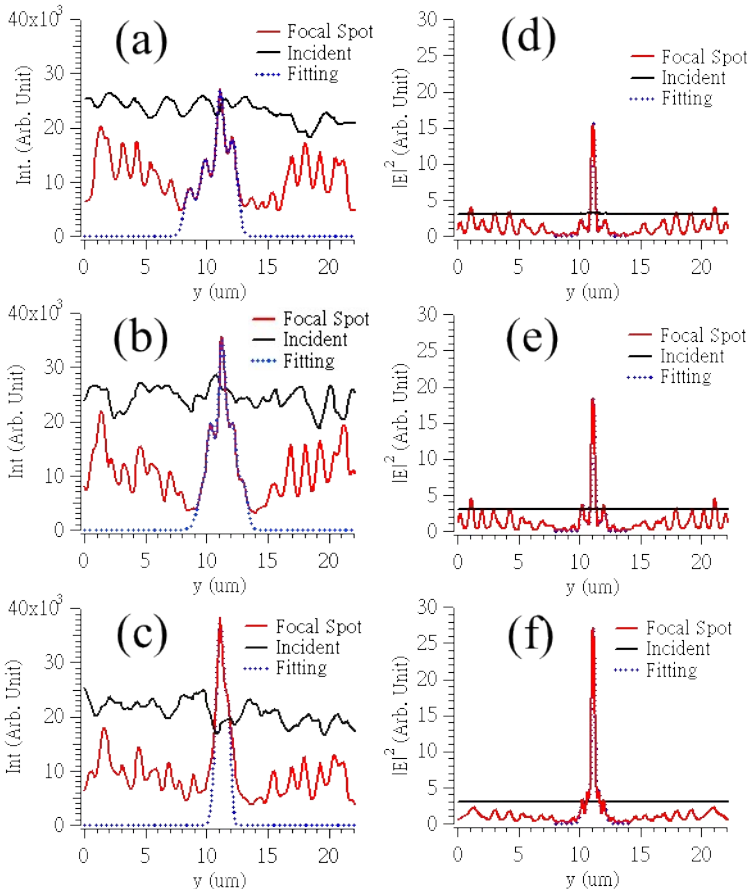

Fig. S8. Intensity line profiles for the calculation of focusing efficiency of the FPZP structures with focal lengths of 5um, (a)-(c) the line profiles from the experimental fluorescent images, (d)-(f) the simulation. (a) and (d) the 2-level FPZP with ideal zone width $\boldsymbol{d}$ = 1.30um, (b) and(e) the 2-level optimized FPZP structure with zone width $\boldsymbol{d}$ = 1.01um. (c) and (d) the optimized 4-level FPZP structure.

The focusing efficiency of an optical devices is defined as the ratio of the power at the focused spot to the total power of the incident light. In our case, the power density is presumed proportional to the fluorescent intensity of the image in the experiment or the E-field intensity $|E|^2$ in the simulation, and the total power is proportional to the area under the intensity line profile extracted from the region of interest. For the power at the focal spot, we first fitted the intensity line profile extracted from the experimental images or simulated $|E|^2$ intensity distribution with multiple Gaussian peaks, and then calculated the area $\boldsymbol{A_f}$ under the central Gaussian peak that corresponds to the peak of the focal spot. For the incident power, we extracted intensity line profile from the same images over the spatial span of the FPZP structure, and numerically integrated the area A_{inc} under the line profile. Finally, we obtained the focusing efficiency with ratio A_f/A_{inc}. We perform the aforementioned procedure with the results of the 2-level FPZP structure with ideal zone width of 1.30 um, the optimized 2-level FPZP structure, and that of the 4-level FPZP structure. The focal length is 5-um for all structures. The line profiles

and the fitted multi-gaussian curves are shown in the figure above, and the focusing efficiency are shown in table 1 in the main text.

VI. Longevity of FPZP Structures

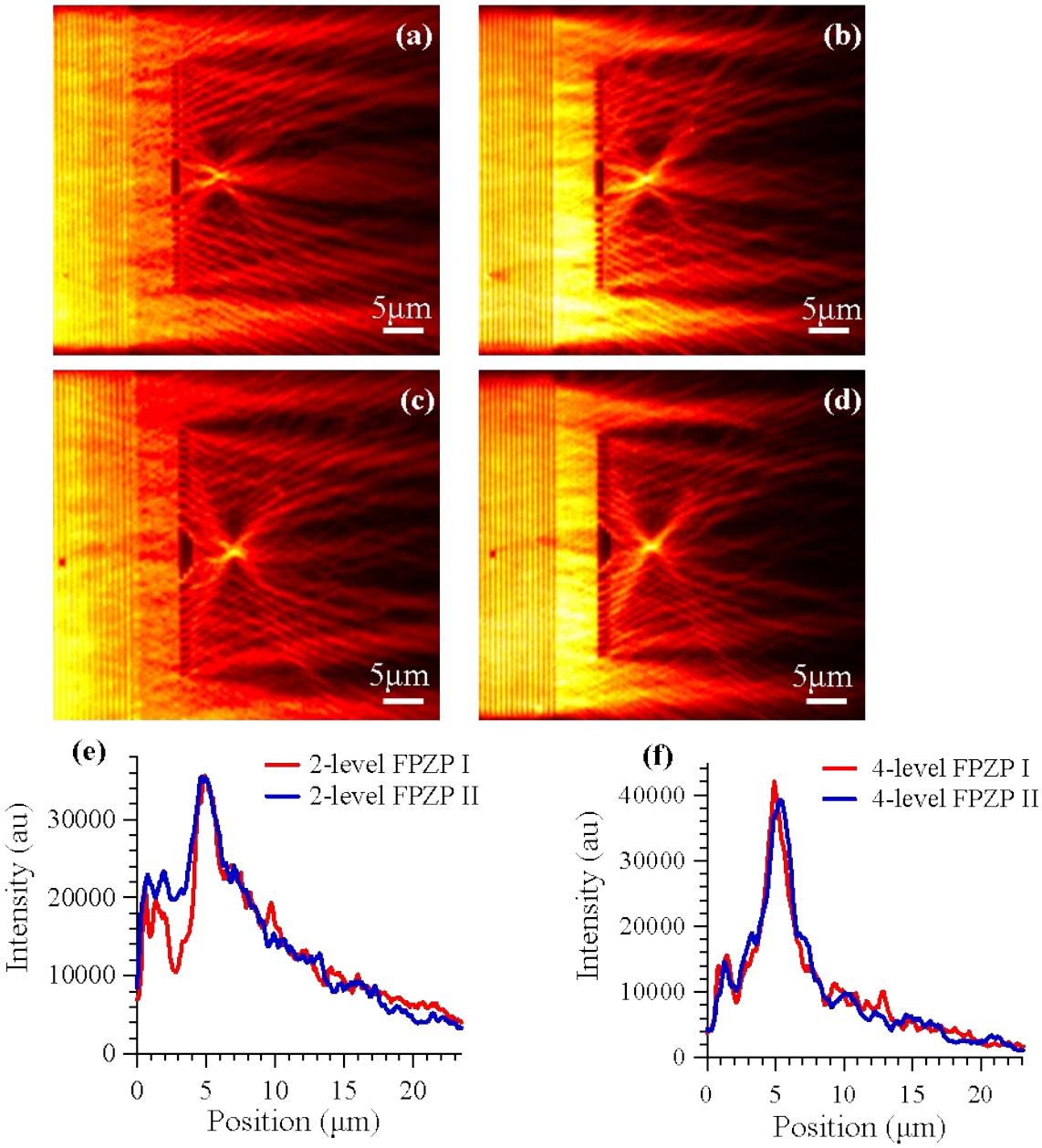

Figure S9 Comparison of upconversion fluorescence microscope images of SPP focusing with FPZP structures recorded ~8 month apart. (a) and (c) the initial images of the SPP focusing with the 2-level and 4-level FPZP structures, respectively. (b) and (d) The SPP focusing with the same 2-level and 4-level FPZP structures, respectively, recorded after ~8 months. The imaging conditions are identical for all the images, and the focal lengths is 5 μm. (e) and (f) the line profiles extracted from the images of the 2-level and 4-level FPZP structure across the focal spot in the longitudinal direction. The red curves represent the intensity line profiles from the initial images, and the blue curves represent the line profiles from the later images.